Published in final edited form as:
Phys Med Biol. 1999 July ; 44(7): 1843–1860.

Simultaneous Technetium-99*m*/Thallium-201 SPECT Imaging with Model-Based Compensation for Cross-Contaminating Effects

Dan J. Kadrmas, Ph.D.[†], **Eric C. Frey, Ph.D.**[‡], and **Benjamin M.W. Tsui, Ph.D.**[‡]

[†]Utah Center of Advanced Imaging Research, Department of Radiology, University of Utah, Salt Lake City, UT 84108

[‡]Department of Biomedical Engineering and Department of Radiology, The University of North Carolina at Chapel Hill, Chapel Hill, NC 27599

Abstract

Simultaneous acquisition of dual-isotope SPECT data offers a number of advantages over separately acquired data; however, simultaneous acquisition can result in cross-contamination between isotopes. In this work we propose and evaluate two frameworks for iterative model-based compensation of cross-contamination in dual-isotope SPECT. The methods were applied to cardiac imaging with Technetium-99*m*-sestamibi and Thallium-201, and they were compared to a subtraction-based compensation method using a cross-talk estimate obtained from an auxiliary energy window. Monte Carlo simulations were performed to carefully study aspects of bias and noise for the methods, and a torso phantom with cardiac insert was used to evaluate the performance of the methods for experimentally acquired data. The cross-talk compensation methods substantially improved lesion contrast and significantly reduced quantitative errors for simultaneously acquired data. Thallium image normalized mean square error (NMSE) was reduced from 0.522 without cross-talk compensation to as low as 0.052 with model-based cross-talk compensation. This is compared to a NMSE of 0.091 for the subtraction-based compensation method. The application of a preliminary model for crosstalk arising from lead fluorescence x-rays and collimator scatter gave promising results, and the future development of a more accurate model for collimator interactions would likely benefit simultaneous Tc/Tl imaging. Model-based compensation methods provide feasible cross-talk compensation in clinically acceptable times, and they may ultimately make simultaneous dual-isotope protocols an effective alternative for many imaging procedures.

I. Introduction

Dual-isotope SPECT studies have a wide range of uses, including the evaluation of myocardial viability and perfusion (Liu *et al.*, 1986; Johnson *et al.*, 1987; Johnson *et al.*, 1990; Alexander and Oberhausen, 1995), brain function (Juni *et al.*, 1992; Devous *et al.*, 1992a, 1992b), lung function (Klumper and Zwijnenburg, 1986), hyperparathyroidism (Sandrock *et al.*, 1990; Neumann, 1992) and others. The radionuclides used for these studies also include a number of combinations, such as Tc-99*m* / Tl-201, Tc-99*m* / In-111, Tl-201 / In-111, Tc-99*m* / I-123, Tc-99*m* / Kr-81*m*, F-18 / Tc-99*m* and others. This paper is developed within the context of simultaneous Tc-99*m*-sestamibi / Tl-201 imaging, with the application of stress/rest myocardial perfusion imaging in mind (Berman *et al.*, 1994; Maddahi *et al.*, 1994). The proposed methods could easily be adapted for use with other isotope combinations and imaging applications.

Send correspondence and reprint requests to: Dan J. Kadrmas, Ph.D., Utah Center of Advanced Imaging Research, Department of Radiology, University of Utah, 729 Arapeen Dr., Salt Lake City, UT 84108-1218, Tel: 801-581-5937, Fax: 801-585-3592.

When performing dual-isotope SPECT imaging, simultaneous acquisition of projection data for both isotopes has a number of advantages over sequential acquisition. The use of one acquisition instead of two doubles the throughput of the hardware and ensures perfect coregistration between the images for each isotope. Patient discomfort is reduced, which in turn reduces the likelihood of artifacts due to patient movement. If such motion artifacts are present, they will affect the images of both isotopes in the same way. Furthermore, simultaneous acquisition allows data for both isotopes to be acquired under identical physiologic conditions. The disadvantage of this approach is that there can be substantial cross-contamination, or 'cross-talk', between the data sets for each isotope. The primary source of cross-talk is down-scatter of higher energy photons from one isotope to the energy window for the other isotope, but in some cases other sources of cross-talk may be important.

In the case of simultaneous Tc-99*m* / Tl-201 imaging, there is substantial cross-talk from Tc into the Tl photopeak energy window in the region of 70–80 keV. This is demonstrated by the sample dual-isotope energy spectrum shown in Figure 1, where the energy windows used in this paper are also indicated. The Tc data is somewhat contaminated by the presence of Tl gammas at 135.3 and 167.4 keV; however, due to the low abundance of these emissions and the high dose ratio of Tc to Tl, the Tl → Tc cross-talk is relatively insignificant. One the other hand, Tc → Tl cross-talk is substantial. The largest component of Tc → Tl cross-talk is down-scatter of 140 keV Tc photons, but a second source of cross-talk is also important—fluorescence x-rays and scatters produced by photons interacting with the collimator (Moore *et al.*, 1994). The Tc → Tl cross-talk can lead to artifacts such as grossly inaccurate quantitation and reductions in defect size and contrast in the Tl image (Kiat *et al.*, 1994;Lowe *et al.*, 1993). For example, when using Tc-99*m*-sestamibi as the stress agent and Tl-201 as the rest agent, the artifacts associated with Tc → Tl cross-talk may cause defect reversibility to be overestimated. Simultaneous Tc / Tl myocardial perfusion imaging is not recommended for clinical use until adequate methods of compensating for cross-talk can be developed (Berman *et al.*, 1994).

A number of researchers have investigated using subtraction-based or restoration-based methods to compensate for the effects of cross-talk in simultaneous Tc-99*m* / Tl-201 imaging (Yang *et al.*, 1993; Knesaurek, 1994; Hademenos *et al.*, 1995; Moore *et al.*, 1995; Links *et al.*, 1996). These methods involve estimating the cross-contamination component and either subtracting or deconvolving the data to yield an uncontaminated result. Only Moore *et al.* specifically included an estimation of the lead fluorescence x-ray contamination in the Tl window. While these methods lead to improvements in quantitation and contrast in the Tl image, they each have disadvantages similar to those associated with single-isotope scatter subtraction methods: each requires *ad hoc* determination of parameters such as scaling factors or blurring functions, the cross-talk estimate may not be accurate for all imaging situations, and the subtraction (or deconvolution) step is accompanied by a large increase in statistical noise. In a phantom evaluation by Cao *et al.* (1996), subtraction-based crosstalk compensation methods were found to overestimate defect size and resulted in increased heterogeneity in the myocardial wall in some situations.

An alternative to using subtraction-based compensation methods is to model the cross-contaminating processes during iterative reconstruction. This approach is closely related to the method of iterative reconstruction-based scatter compensation (RBSC) (Frey and Tsui, 1993; Frey *et al.*,, 1993; Beekman *et al.*, 1993, 1994; Floyd *et al.*, 1995; Welch *et al.*, 1995). Previous research with RBSC has demonstrated that it can provide images with both less bias and reduced noise (Frey *et al.*,, 1992; Kadrmas *et al.*, 1997; Beekman *et al.*, 1997) as compared to subtraction-based scatter compensation methods. Though RBSC is computationally more demanding than subtraction-based compensation, recent advances in scatter models (Frey and Tsui, 1996) and fast implementation methods (Kadrmas *et al.*, 1998a) have greatly reduced

these demands. Presently, iterative RBSC can be performed with reconstruction times that are only nominally greater than similar reconstructions without scatter compensation, and with modern workstations these reconstruction times are clinically acceptable.

In this work we propose and evaluate two methods for the iterative reconstruction of simultaneously acquired dual-isotope data that use model-based methods to compensate for the effects of cross-talk. One of these methods is directly related to RBSC, and the other is a hybrid of subtraction and RBSC which uses model-based estimation of the cross-talk component. An energy-based subtraction correction method, similar to that proposed by Moore *et al.*, was also studied for comparison. It is intended to provide an example of the relative performance for the subtraction-based class of crosstalk compensation methods. The methods were evaluated using both Monte Carlo simulated and experimentally acquired phantom data, and comparisons are made to the cases of separate acquisition (no cross-talk) and simultaneous acquisition without compensation.

II. Methods

A. Cross-talk compensation methods

Three compensation methods are studied in this work. The first method, called 'triple window compensation' (TWC), is an energy window-based subtraction correction method similar to the method previously developed by Moore *et al.* (1995). The other two compensation methods studied are new methods based upon modeling the effects of cross-contamination. These methods are called simultaneous and sequential model-based compensation (SimMBC and SeqMBC, respectively).

i) Triple window compensation—The TWC method is essentially Moore's method extended for use with iterative reconstructions. As proposed, the method pre-corrected the Tl energy window data for cross-talk before performing a filtered-backprojection reconstruction. No compensation was performed for the less substantial contamination of the Tc data. We have extended the method for use with iterative reconstructions. When performing iterative reconstruction, the cross-talk estimate can be added to the forward projection in order to achieve compensation (Lange and Carson, 1984; Bowsher *et al.*, 1996). This is similar to performing a pre-reconstruction subtraction, but it has the advantage that it preserves the Poisson statistics of the projection data.

The TWC method consists of acquiring an intermediate "scatter" window in addition to the Tl and Tc photopeak energy windows. This intermediate energy window is placed just above the Tl energy window at 90–110 keV as shown in Figure 1. Moore *et al.* found that the cross-talk component in the Tl energy window (c_{Tl}) could be approximated by scaling the data acquired in the Tc photopeak (w_{Tc}) and intermediate (w_{int}) energy windows and convolving them with blurring functions:

$$c_{Tl} = k_1 w_{Tc} \otimes g_1 + k_2 w_{int} \otimes g_2 \quad (1)$$

where k_1, k_2, g_1 and g_2 are scaling and Gaussian blurring functions for the Tc and intermediate energy windows, respectively. The data acquired in the intermediate window accounts primarily for the down-scatter component of the cross-talk, and the blurred data from the Tc photopeak window accounts primarily for the lead fluorescence x-ray component of the cross-talk. The scaling and blurring functions attempt to transform the number and spatial distribution of the crosstalk estimate to match the actual crosstalk component acquired in the Tl energy window.

The scaling and blurring parameters for the TWC method are determined empirically. Since the parameters are not based upon the imaging physics, assumptions must be made as to the optimal values of these parameters for different imaging situations. For the simulation experiment, which did not include fluorescence x-rays, the blurring and scaling factors were optimally chosen to minimize the mean squared error between the TWC estimate and the true cross-talk component. Using such optimized parameters results in the upper limit on performance for the TWC method. For the experimentally acquired data, the parameters used by Moore were adjusted to account for the slightly different energy windows used in this study. Thus, the TWC parameters were not specifically optimized for the experimental data, but rather represented what could reasonably be expected for general use of the method.

ii) Simultaneous model-based compensation—The SimMBC method is based upon modeling the effects of cross-contamination during the reconstruction process. The method is called *simultaneous* model-based compensation since the images for the two isotopes are reconstructed simultaneously from the multiple energy window projection data. The maximum-likelihood expectation-maximization (MLEM) algorithm (Lange and Carson, 1984; Shepp and Vardi, 1982) using SimMBC for dual-isotope SPECT looks nearly identical to the MLEM algorithm using RBSC for single-isotope SPECT. The differences for SimMBC are that the number of reconstructed image voxels spans the images for both isotopes, the number of measured data points spans the multiple energy window data set, and the projection and backprojection matrices describe all possible image-to-projection interactions, including cross-talk. The equation for the MLEM image update using SimMBC is:

$$\widehat{x}_i^{n+1} = \widehat{x}_i^n \frac{1}{\sum_{j=1}^{2M} F_{ji}} \sum_{l=1}^{2M} \frac{F_{li}\tilde{p}_l}{\sum_{k=1}^{2N} F_{lk}\widehat{x}_k^n}, \tag{2}$$

where N is the number of voxels in each image and M is the length of the projection data vector for each energy window. In this representation, the reconstructed image vector $\hat{\mathbf{x}}$ is a concatenation of the separate image vectors for each isotope, so it has length $2N$; likewise, the projection data vector $\tilde{\mathbf{p}}$ is a concatenation of the data vectors for each energy window, so its length is $2M$.

The projection matrix $\mathbf{F}$ models the physics of the data acquisition process. For quantitatively accurate results, these models should include the effects of non-uniform attenuation, depth-dependent detector-response, scatter, and all sources of cross-talk. Additionally, the energy-dependent camera sensitivity, energy resolution, and detection efficiency in each energy window are modeled. For isotopes such as Tl-201 that have multiple emission energies, the relative abundance and detection efficiency for each emission are also modeled.

The projection matrix is $2M \times 2N$ and can be divided into four quadrants: $\mathbf{F}_{\mathrm{Tc}\rightarrow\mathrm{w(Tc)}}$, $\mathbf{F}_{\mathrm{Tc}\rightarrow\mathrm{w(Tl)}}$, $\mathbf{F}_{\mathrm{Tl}\rightarrow\mathrm{w(Tc)}}$ and $\mathbf{F}_{\mathrm{Tl}\rightarrow\mathrm{w(Tl)}}$, where the subscripts indicate the image-to-energy window projection represented by each quadrant. This is shown graphically in Figure 2. The physics of the cross-talk are included in the off-diagonal quadrants; *e.g.*, $\mathbf{F}_{\mathrm{Tc}\rightarrow\mathrm{w(Tl)}}$ should include models for both down-scatter of Tc photons into the Tl photopeak energy window, and fluorescence x-rays produced by Tc photons interacting with the collimator that are collected in the Tl photopeak window. Likewise, $\mathbf{F}_{\mathrm{Tl}\rightarrow\mathrm{w(\ Tc)}}$ includes the contribution of the 135 and 167 keV Tl gammas to the data acquired in the Tc photopeak window. By modeling the cross-talk in $\mathbf{F}$, reconstruction-based cross-talk compensation is performed. Furthermore, scatter from each isotope into its own photopeak energy window is modeled so that self-scatter RBSC is also performed.

In order to compensate for cross-talk with SimMBC, all isotope-to-energy window combinations need to be included in the projection step. However, all such combinations do not necessarily need to be included in the backprojection step—backprojections from non-photopeak energy windows can be excluded. This results in using unmatched projector/backprojector pairs, which have been shown in practice to reconstruct nearly the same images as matched projector/backprojector pairs, but in much shorter reconstruction times (Kamphuis *et al.*, 1998). In (Kadrmas *et al.*, 1997) it was found that including non-photopeak energy windows in single-isotope reconstructions led to minor reductions in variance, but at the cost of increased reconstruction times. We performed a preliminary investigation into dual-isotope imaging with SimMBC and obtained similar results. If accurate cross-talk models are used, then the best reconstruction is expected to result when all isotope-to-energy window combinations are included in both the projection and backprojection steps; however, nearly as good performance can be obtained in much shorter reconstruction times by excluding non-photopeak energy window backprojections. Practical implementations of SimMBC need include only backprojections from the corresponding photopeak energy windows. Equation (2) was written with a matched projector / backprojector pair that includes all isotope-to-energy window combinations. The algorithm can be modified to exclude backprojections from non-photopeak energy windows by zeroing the $\mathbf{F}_{\mathrm{Tc}\rightarrow\mathrm{w(Tl)}}$ and $\mathbf{F}_{\mathrm{Tl}\rightarrow\mathrm{w(Tc)}}$ quadrants during the backprojection. Further details on the fast implementation methods used in this paper can be found in section *II.B.* below.

iii) Sequential model-based compensation—The SimMBC method potentially offers the most accurate cross-talk compensation of the methods studied. However, modeling cross-talk during simultaneous reconstruction is computationally demanding. A faster model-based compensation method can be used in the case of simultaneous Tc / Tl imaging. Since the Tc photopeak energy window data contains relatively little cross-contamination, the Tc image can be reconstructed without cross-talk compensation. The cross-talk in the Tl energy window can then be estimated by projecting the reconstructed Tc image into the Tl energy window (*i.e.*, using $\mathbf{F}_{\mathrm{Tc}\rightarrow\mathrm{w(Tl)}}$). The Tl image is then reconstructed using the projected cross-talk estimate for compensation by adding it to the forward projection step as in the TWC method. Since the Tc and Tl images are reconstructed sequentially, the method is called sequential model-based compensation. The major steps for reconstruction with SeqMBC are:

1. Reconstruct the Tc image with self-scatter compensation (cross-talk compensation not required).
2. Estimate the cross-talk in the Tl energy window by down-projecting the reconstructed Tc image with models for cross-contamination.
3. Reconstruct the Tl image, using the cross-talk estimate from the previous step for compensation.

When using SeqMBC (or SimMBC) it is important to perform self-scatter compensation when reconstructing the Tc image. If this is not done, the quantitative inaccuracies in the Tc image due to scatter can propagate through the Tc→Tl window projection, leading to an inaccurate cross-talk estimate. Since both of these algorithms are well suited for use with self-scatter RBSC, this does not pose a problem.

B. Experimental methods

The cross-talk compensation methods were evaluated using both Monte Carlo simulated data and experimentally acquired data of a physical phantom. In both cases, the images were compared to (*i*) images reconstructed from separately acquired data ('no cross-talk') and (*ii*) images reconstructed from simultaneously acquired data without cross-talk compensation ('no compensation'). The details of the simulated and experimental acquisitions are given below.

i) Simulated phantom experiment—The simulated phantom experiment used the 3D MCAT phantom (Terry *et al.*, 1990; Tsui *et al.*, 1994) shown in Figure 3. The phantom torso was 36 cm wide, 24 cm deep, and 40 cm long. The phantom was digitized onto a 64^3 image matrix using 0.625 cm cubic voxels. Two activity distributions were described for the phantom, one for Tc-99*m*-sestamibi and the other for Tl-201. The relative activity concentrations ratios myocardium:liver:body:lungs were 71:71:5:10 for Tc and 43:19:2:1 for Tl. Note that these numbers do not reflect the Tc:Tl activity ratio, which is discussed below. No lesions were present, and blurring due to the MCAT phantom 'beating heart' model was included (Pretorius *et al.*, 1997). Using these phantoms, the simulations for Tc and Tl were performed separately, allowing the data sets to be added later to imitate simultaneously acquired data.

The SIMIND Monte Carlo program (Ljungberg and Strand, 1989) was used to simulate 1.1×10^{10} photon histories, providing a data set with low simulation noise. The camera was equipped with a LEGP parallel hole collimator, and the energy resolution was 10% FWHM at 140 keV and varied as $1/\sqrt{\text{energy}}$. The scan consisted of 64 evenly spaced projection views acquired over a 180° arc from 45° LPO to 45° RAO. A 64×64 projection matrix with 0.625 cm bins was used, and the data were binned into the energy windows shown in Figure 1 (64–88 keV for Tl photopeak, 126–154 keV for Tc photopeak, and 90–110 keV for the intermediate TWC energy window). The simulation included the 3D effects of non-uniform attenuation, depth-dependent detector response and Tc→Tldown-scatter (up to 10 orders of scatter, both coherent and incoherent). Due to limitations of the Monte Carlo code, the effects of Pb fluorescence x-rays and collimator scatter were not simulated.

The simulated projection data were scaled and Poisson noise added to correspond to scans which acquired 1.60×10^5 Tc counts per typical cardiac slice in the Tc photopeak energy window, and 6.0×10^4 Tl counts per typical cardiac slice in the Tl photopeak energy window. At these count levels, there were about 8.0×10^4 counts per slice down-scattered from Tc into the Tl energy window. Notice that this was a very large amount of Tc→Tl cross-talk—more than the number of Tl counts—and a rather low count level; clinically somewhat higher counts and lesser relative amounts of cross-talk could be expected. This severe level of cross-talk presents a demanding test of the compensation methods being evaluated.

The simulation experiment was designed to specifically address the issue of down-scatter contamination from Tc into the Tl energy window. As such, the only scattered photons included in the simulation were those down-scattered from Tc, and no fluorescence x-rays or collimator scatter were included. 'Perfect' self-scatter rejection was assumed, meaning no scatter from either isotope into its own energy window was included. The simulated data sets included primary photons from Tc and Tl in each energy window, and Tc→Tl down-scattered photons.

ii) Anthropomorphic phantom experiment—Experimentally acquired data were used to realistically evaluate the proposed compensation methods in the presence of self-scatter, down-scatter and lead fluorescence x-ray contamination. A 36× 28 cm plastic and water anthropomorphic phantom with cardiac insert was used (Data Spectrum, Hillsborough, N.C.). The phantom was imaged on a GE Optima dual-head SPECT system equipped with a Gd-153 scanning line source for transmission measurements. A LEGP parallel hole collimator was used, and 128 evenly spaced views were acquired over 360° for each scan. Separate scans were acquired for Tc and Tl, and each scan acquired data in all the energy windows shown in Figure 1.

The phantom was first assembled with a single cold lesion placed somewhat basally in the septal wall. It was filled with a Tc distribution of 15:15:1 in the myocardium:liver(bowel):body and imaged (no activity was placed in the lungs for either the Tc or Tl experiments). About 3.50×10^5 counts were acquired per typical cardiac slice in the Tc photopeak window. Since

this count level was somewhat higher than desired, the Tc data were pruned down by a factor of 1/3 electronically (this was done in a statistically accurate manner with a random number generator in order to maintain the Poisson statistical nature of the projection data). The resultant data set had about 2.50×10^5 counts per cardiac slice in the Tc photopeak window, and 1.90×10^5 contaminant counts per slice in the Tl energy window. The Tc was allowed to decay for several days, and a second cold lesion was placed in the inferior mid-ventricular wall close to the liver. This lesion placement was chosen to maximize scatter effects from the liver. The phantom was then filled with a Tl-201 activity distribution of 20:10:1 myocardium:liver (bowel):body, carefully repositioned in the gantry, and imaged. The Tl scan acquired about 1.20×10^5 counts per cardiac slice in the Tl photopeak window (1.5×10^4 contaminant counts per slice in the Tc photopeak window). The data from the two scans were later added to imitate a simultaneous dual-isotope acquisition with a single Tc lesion and two Tl lesions. Note that there was a very high degree of Tc→Tl cross-talk for this experiment, again presenting a demanding challenge for the compensation methods being evaluated.

C. Reconstruction methods

All reconstructions were performed using ordered-subsets (Hudson and Larkin, 1994) with four angles per subset. The angles within subsets were evenly spaced along the camera orbit, and successive subsets were ordered to maximize the angular distance between subsets. The reconstruction program used a rotation-based projector and backprojector pair (Zeng and Gullberg, 1992). The 3D effects of non-uniform attenuation and depth-dependent detector response were modeled in both the projector and backprojector at all iterations.

i) Scatter model—When applicable, scatter was modeled in the projector using the effective source scatter estimation (ESSE) model (Frey and Tsui, 1996). The ESSE model accounts for the spatial-variance and object-dependence of scattered photons, and it can be calibrated for many orders of scatter, making it suitable for modeling down-scatter across a wide energy range. Pertinent factors included in the models include the energy-dependence of the scatter response function, the energy-dependent detector sensitivity and resolution, the energy window settings, coherent and incoherent scatters, and so on. Also note that the ESSE model accounts for most, but not all, of the effects of non-uniform scattering media. The ESSE scatter model must be calibrated for the emission energy(ies) and acquisition windows of interest before it can be applied. This was done for each isotope using a modified version of the SIMIND Monte Carlo code. The more involved calibrations specific for Tl-201 imaging are given in (Kadrmas *et al.*, 1998b). Up to 10 orders of scatter were included in the calibration simulations, which was found to be sufficient to model down-scatter from Tc to the Tl energy window.

The scatter model was implemented using the fast implementations described in (Kadrmas *et al.*, 1998a); pertinent details include a coarse-grid collapse factor of 2.0 and “Intermittent RBSC” for the first two iterations. For the TWC and SeqMBC methods, the cross-talk estimate was added to the forward projection during the Tl reconstruction to enable compensation (Lange and Carson, 1984Bowsher *et al.*, 1996). For the experimental reconstructions, self-scatter (scatter from one isotope into its own photopeak energy window) was modeled in all cases; *i.e.*, self-scatter RBSC was performed. Self-scatter RBSC was not performed for the MCAT phantom reconstructions since self-scatter was excluded from those simulations.

ii) Preliminary model for collimator interactions—The development of a detailed model for lead fluorescence x-rays and collimator scatter is beyond the scope of this work. We have applied a preliminary model for these effects and incorporated it into the crosstalk model for Tc→Tlenergy window interactions. This preliminary model is based upon the approximation that the cross-talk due to fluorescence x-rays and collimator scatter is proportional to the Tc photopeak image. Under this assumption, contamination in the Tl

photopeak window due to collimator interactions is modeled as being a scaled version of the photons (primary+scatter) in the Tc photopeak window blurred by a Gaussian.

The scaling and blurring factors were empirically determined from a simulation of a Tc point source placed on the axis of a 22 cm diameter water-filled cylinder. The MCNP4B Monte Carlo code (Los Alamos National Laboratory) was used to simulate acquisition of planar images into both the Tc and Tl photopeak energy windows. A LEGP parallel hole collimator with round holes and lead septa was simulated, and photons were tagged according to interactions within the patient and/or collimator. The contribution in the Tl energy window due to fluorescence x-rays and collimator scatter was summed and found to represent 18% of the crosstalk events, a result in accordance with other studies (Moore *et al.*, 1994; O'Connor *et al.*, 1998). For the purposes of the preliminary model, the ratio of crosstalk x-rays and collimator scatter to the total counts in the Tc window was found to be 0.209. The preliminary model used here was sufficient to allow evaluation of the model-based compensation methods using experimental data. Given our experiences in this work, it is apparent that the development of a more detailed model based upon modeling the physics of fluorescence x-rays and collimator scattering would be beneficial. Such a model would obviate the need for a *ad hoc* scaling and blurring parameters, and it could potentially reduce the bias associated with the cross-talk compensation methods demonstrated later in this paper.

iii) Data processing—The reconstructions from noisy data were displayed after being post-processed with a Butterworth filter of order 5 and cut-off 0.3 cm^{-1}. The noise levels arising from each of the methods were studied in detail for the simulated MCAT experiment. This was done by reconstructing 100 independent noise realizations of the simulated data and computing the population variance image for each compensation method. To facilitate computation of the variance images, these reconstructions were carried out in 2D; however, the 3D effects of scatter were accounted for in this analysis by assuming a line-source geometry. No Butterworth filtering was applied in the computation of the variance images.

III. Results

A. MCAT simulation experiment

The MCAT phantom simulation experiment was designed to study the effects of Tc→Tl down-scatter compensation. The noise-free reconstructed short-axis thallium images for each of the methods studied are shown in Figure 4. The images of Figure 4 demonstrate gross artifacts for the no compensation images, and substantial reductions of these artifacts are seen for each of the proposed compensation methods. The target images here are the 'no cross-talk' images (bottom row), which correspond to separately acquired data.

The differences in the compensated images can be seen more easily by looking at the polar maps shown in Figure 5. Relative error polar maps were calculated by subtracting the 'no cross-talk' polar map from the polar map for each other case, then dividing the result by the 'no cross-talk' polar map. The relative error polar maps show that the uncorrected dual-isotope reconstruction resulted in as much as an 86% overestimation of intensity in the Tl image, but these errors were reduced to the range of −8% to +15% for the compensated images. The TWC method resulted in a slight overestimation of image intensity in the septal wall and a slight underestimation in the inferior wall, whereas opposite effects were seen for the model-based methods. These differences can be attributed to different biases in the cross-talk estimates for each of the compensation methods. Recall that the TWC parameters were specifically optimized for the simulated data; in practice such optimization could not be achieved, and somewhat poorer performance could be expected.

The Tl images reconstructed from the noisy projection data are shown in Figure 6, along with the reconstructed variance images for the same transaxial slice. Some qualitative differences in noise level and texture can be seen in these images. In order to further evaluate the noise properties of the methods, we have calculated measures of mean-variance and contrast for each image. Plotting variance versus contrast helps ensure that the noise levels are compared at similar degrees of iterative convergence, and the relationship between variance and contrast can in some sense be considered a measure of signal-to-noise. The mean-variance for each image was calculated by averaging over all voxels. Likewise, the myocardium-to-chamber contrast ratio was calculated by drawing ROIs over the myocardium and chamber in the noise-free reconstructions. The contrast ratio was defined as (MY−CH)/(MY+CH), where MY and CH represent the average voxel values in the myocardium and chamber ROIs, respectively.

The results of the variance versus contrast analysis are plotted in Figure 7. Individual pixels throughout the myocardium were tested for differences in variance using the variance ratio test (Zar, 1996). No statistically significant differences in noise levels were found between any of the compensation methods. However, in all cases, the images for simultaneously acquired data resulted in significantly higher noise levels than did the separately acquired ‘no cross-talk’ images ($p < 0.05$). This noise increase is analogous to that associated with scatter and its compensation in single-isotope imaging. The presence of cross-talk in the simultaneously acquired projection data increases the contamination counts in the Tl window. Though one can correct for the bias arising from the contamination component, the noise component cannot be eliminated and will always propagate to the reconstructed image. This noise increase can be controlled using regularization methods such as linear filtering or Bayesian reconstruction methods, but a greater degree of regularization will be required for simultaneously acquired data as compared to separately acquired data.

There are several ways in which the noise in the Tl window data can be reduced. First, the ratio of Tc dose to Tl dose can be reduced, thereby reducing the Tc→Tl contamination component and its contribution to noise. This approach leads to a corresponding increase in noise in the Tc data, which may not be acceptable. Some gains may also be realized by optimizing the Tl energy window for simultaneous imaging. Finally, a significant reduction in the noise in the Tl data could result from hardware improvements; *e.g.*, by improving the energy resolution of the camera to gain better scatter rejection capability. The impact of increased noise in simultaneously acquired dual-isotope data must be addressed before simultaneous acquisition protocols should be considered for clinical use. The greater degree of regularization required to control these higher noise levels may introduce additional bias into the images, and the impact of this upon lesion detection should be investigated.

B. Anthropomorphic phantom

The experimentally acquired phantom data were used to evaluate the ability of the methods to compensate for cross-talk in the more realistic situation where self-scatter and collimator interactions were present. Recall that, in this experiment, there was a lesion in the basal portion of the septal wall for both Tc and Tl, and an additional Tl lesion was placed in the inferior mid-ventricular wall. The second Tl lesion was placed close to the liver to maximize scatter from the liver, and cross-talk effects should be most severe here since there was no corresponding Tc lesion in this location. Such a lesion present for Tl but not for Tc would not be expected to be seen clinically when Tl is the resting agent and Tc the stress agent, but it does present a very challenging situation as far as cross-talk compensation is concerned.

Reconstructed short-axis Tc images for the phantom experiment are shown in Figure 8. Six iterations of OSEM were used for all cases. Note that, since TWC and SeqMBC do not include compensation for the Tl →Tc cross-talk, they result in the same Tc images as ‘no cross-talk compensation’. The images of Figure 8 do not show significant cross-talk effects, but there

was an overestimation of counts and slight loss of contrast in the uncompensated Tc images. The SimMBC method successfully compensated for the small degree of cross-talk in the Tc energy window, resulting in images very similar to the 'no cross-talk' images. We conclude that, while Tl →Tc cross-talk is not a significant concern, the SimMBC method does provide compensation for this effect.

The effects of Tc→Tl cross-talk and its compensation can be assessed from the images shown in Figure 9 and Figure 10. All of the compensation methods provided substantial improvements in image quality as compared to the no compensation images. The lesion in the basal portion of the septal wall can be easily seen in all cases, and this lesion had better contrast and was better defined in the compensated images than in the uncompensated image. The more difficult lesion placement, in the inferior mid-ventricular wall, was clearly visualized only in the 'no cross-talk' images. Visualization of the lesion was difficult at best in the simultaneously acquired Tl images, though the contrast of the lesion was somewhat improved in each of the compensated images as compared to the uncompensated image.

The relative error polar maps of Figure 10 demonstrate that none of the compensation methods fully recovered the lesion contrast. The importance of including compensation for collimator interactions can also be seen in Figure 10: without the x-ray model, both SimMBC and SeqMBC underestimated the cross-talk component, resulting in an overestimation of Tl image intensity; however, when the x-ray model was used, both model-based compensation methods provided images with higher defect contrast and pixel values much closer to the true values. The relative error polar maps also demonstrate somewhat greater non-uniformity in the error distribution for the TWC method as compared to the model-based compensation methods. Such non-uniformities may contribute to an increased likelihood of false-positive readings due to cross-talk artifacts.

Image quality was further evaluated using quantitative measures of lesion contrast and normalize mean square error (NMSE). For each lesion, the contrast ratio was calculated by drawing ROIs over the lesion and neighboring myocardial wall. The contrast ratio was defined as (MY−LS)/(MY+LS), where MY and LS represent the mean voxel value in the myocardial and lesion ROIs, respectively. For the Tc reconstructions, the lesion contrast was reduced by 6.2% due to the presence of Tl → Tc crosstalk. The only method studied that compensated for Tl → Tc crosstalk was SimMBC, which restored the contrast of the Tc lesions to within 0.7% of its separately acquired value.

The contrast ratios for the Tl lesion placed in the basal septal wall are plotted as a function of iteration in Figure 11; similar trends were seen for the relative contrast of the Tl lesion in the inferior mid-ventricular wall (not shown). In addition to describing the contrast levels achieved by each method, Figure 11 also provides a sense of the rate at which contrast is recovered with iteration. Each of the crosstalk compensation methods improved lesion contrast as compared to the uncompensated case, with both of the model-based methods outperforming the TWC method. However, at later iterations, the SeqMBC method overestimated the lesion contrast as compared to the no crosstalk data. This is because the SeqMBC method did not compensate for Tl → Tc crosstalk, but used the reconstructed Tc image to predict the Tc→Tl crosstalk. The Tl → Tc crosstalk increased the voxel values in the Tc image, which propagated to the Tc→Tl crosstalk estimate, thereby over-compensating and artificially increasing Tl lesion contrast. This effect could potentially lead to an underestimation of defect reversibility in clinical applications.

The normalized mean square error for the uncompensated image with respect to the 'no cross-talk' image was 0.522. The NMSE was 0.091 when using the TWC method. Without modeling collimator interactions, the SimMBC and SeqMBC methods resulted in NMSEs of 0.113 and

0.053, respectively; however, use of the preliminary model for collimator interactions reduced the NMSEs to 0.075 for SimMBC and 0.052 for SeqMBC. These results demonstrate the importance of compensating for fluorescence x-rays and collimator scatter in simultaneous Tc-99*m* / Tl-201 imaging. They also show that, when using a preliminary model for collimator interactions, the performance of the model-based compensation methods was better than that of the energy-based compensation method. Since the definition of the inferior-wall Tl lesion in the compensated images did not approach that of the 'no cross-talk' image, it is likely that future development of more accurate models for collimator interactions would lead to improved cross-talk compensation. The preliminary model used here was neither fully evaluated nor based in physics, and represents a likely source of error for the model-based compensation methods.

IV. Discussion

Each of the cross-talk compensation methods studied in this paper have desirable and undesirable qualities. The TWC method was perhaps the simplest of the methods studied since it uses energy-based cross-talk estimation as opposed to model-based estimation. The advantages of the TWC method, then, are that it is both fast and easy to apply. The disadvantages of the TWC method are that it requires acquisition of an additional energy window, it requires *ad hoc* determination of scaling and blurring parameters that may change for different imaging situations, and, since the method is not based upon the imaging physics, it is difficult to predict the performance for different imaging situations. This method was chosen for comparison in this work in order to provide an example of a class of subtraction-based compensation methods that have been used by other authors.

The model-based compensation methods behaved similarly to each other, with both SimMBC and SeqMBC providing good compensation with slightly lower noise levels than the TWC method. These methods have the advantages that they do not require determination of scaling or blurring parameters (our preliminary model for collimator interactions does require such a parameter, but the intent is to develop a future model, based in physics, that overcomes this requirement), and they are firmly based in physics. The SimMBC method has the additional advantage that it compensates for Tl → Tc cross-talk, though this source of cross-talk can be expected to be minor for most imaging situations.

The disadvantage of the model-based compensation methods lies in the complexity of the models used. Accurately modeling multiple orders of scatter in inhomogeneous media is not a trivial task, and such modeling is often computationally demanding. Also, a well-grounded model for lead fluorescence x-rays and collimator scatter is not currently available. Recent advances in scatter model development and fast implementation methods have greatly mitigated the first problem (Kadrmas *et al.*, 1998a). In this work we used fast implementations of RBSC and the ESSE scatter model, resulting in reconstruction times that were clinically acceptable for all methods. Reconstructing six OSEM iterations of 28 slices of 64 × 64 images for *both* isotopes from 64 bin × 28 slice × 64 angle projection data took 7.5 c.p.u. minutes on a Digital Personal Workstation 500au (cost ~$6,000) when performing 3D attenuation, detector response and self-scatter compensation. This was our baseline for reconstruction time comparison (corresponding reconstructions without self-scatter RBSC required 5.9 min. total for both isotopes). Dual-isotope reconstruction with cross-talk compensation took the following for the various methods: 7.6 min. for TWC, 8.4 min. for SeqMBC, and 12.3 min. for SimMBC.

The SimMBC method potentially provides the best performance for cross-talk compensation, though it does require somewhat longer reconstruction times than for the SeqMBC method. When reconstruction time is a primary concern, the SeqMBC method may be preferable. Keep

in mind, however, that the SeqMBC method is only applicable when the data for one of the isotopes is largely uncontaminated by the presence of the other. The SimMBC method has no such limitation, and thus is applicable to a wider range of isotope combinations.

It was mentioned previously that the development of an improved model, based upon the principles of physics, for fluorescence x-rays and collimator scatter is an important area for future work. In particular, the assumption of our preliminary model that the contamination due to collimator interactions is proportional to the image in the Tc-99*m* window may be a significant source of error. It is likely that this contamination would be significantly more blurred than the image in the Tc-99*m* energy window. This would have a large impact on the lesion contrast in the phantom experiment due to the proximity and activity of the liver, and would have resulted in undercompensation in regions of the heart near the liver.

V. Summary and Conclusions

We have proposed two model-based cross-talk compensation methods for dual-isotope SPECT imaging, and compared their performance to a previously proposed energy-based compensation method. The methods were evaluated using simulated and experimentally acquired data of simultaneous Tc-99*m* / Tl-201 cardiac imaging which had very high levels of cross-talk, and the bias and noise properties of the methods were studied systematically. All three methods provided significant qualitative and quantitative improvements for simultaneously acquired data, but their effects upon lesion detectability and observer performance have yet to be investigated. The model-based compensation methods provided very accurate compensation in the absence of cross-talk due to fluorescence x-rays and collimator scatter. The application of a preliminary model for these effects gave promising results, though further development is required in this area. Using the preliminary x-ray model, both SimMBC and SeqMBC outperformed the subtraction-based method in term s of lesion contrast and normalized mean square error. In all cases, simultaneously acquired data resulted in significantly higher noise levels in the Tl image than did separately acquired data. As a result, additional regularization may need to be applied to simultaneously acquired data, and the corresponding bias-variance tradeoff should be investigated. The proposed methods are based on existing and well grounded scatter compensation techniques, and they are applicable to a range of isotope combinations other than the one studied here. The model-based methods provide feasible cross-talk compensation in clinically acceptable times, and such an approach may ultimately make simultaneous dual-isotope protocols an effective alternative for many imaging procedures.

Acknowledgments

This work was supported by a grant # R29-CA63465 from the National Cancer Institute and by an academic research grant from the North Carolina Supercomputer Center. Its contents are solely the responsibility of the authors and do not necessarily represent the official views of the National Cancer Institute or the NCSC.

References

Alexander C, Oberhausen E. Myocardial scintigraphy. Sem Nucl Med 1995;25:195–201.

Beekman FJ, Eijkman E, Viergever MA, Borm G, Slijpen E. Object shape dependent PSF model for SPECT imaging. IEEE Trans Nucl Sci 1993;40:31–39.

Beekman FJ, Kamphuis C, Viergever MA. Improved SPECT quantitation using fully three-dimensional iterative spatially variant scatter response compensation. IEEE Trans Med Imag 1996;15:491–499.

Beekman FJ, Kamphuis C, Frey EC. Scatter compensation methods in 3D iterative SPECT reconstruction: a simulation study. Phys Med Biol 1997;42:1619–1632. [PubMed: 9279910]

Berman DS, Kiat H, Train KV, Friedman JD, Wang FP, Germano G. Dual-isotope myocardial perfusion SPECT with rest thallium-201 and stress Tc-99*m* sestamibi. Card Clin 1994;12:261–270.

Bowsher JE, Johnson VA, Turkington TG, Jaszczak RJ, Floyd CE, Coleman RE. Bayesian reconstruction and use of anatomical a priori information for emission tomography. IEEE Trans Med Imag 1996;15:673–686.

Cao Z, Chen CC, Maunoury C, Holder LE, Abraham TC, Tehan A. Phantom evaluation of simultaneous thallium-201/technetium-99m acquisition in single-photon emission tomography. Eur. J. Nucl. Med 1996;23:1514–1520. [PubMed: 8854851]

Devous MD, Payne JK, Lowe JL. Dual-isotope brain SPECT imaging with Tc-99m and I-123: clinical validation using Xe-133 SPECT. J. Nucl. Med 1992a;33:1919–1924. [PubMed: 1432149]

Devous MD, Lowe JL, Payne JK. Dual-isotope brain SPECT imaging with Tc-99*m* and I-123: validation by phantom studies. J Nucl Med 1992b;33:2030–2035. [PubMed: 1432168]

Floyd CE, Jaszczak RJ, Coleman RE. Inverse Monte Carlo: a unified reconstruction algorithm. IEEE Trans Nucl Sci 1995;32:779–785.

Frey, EC.; Tsui, BMW.; Ljungberg, M. A comparison of scatter compensation methods in SPECT: subtraction-based techniques versus iterative reconstruction with accurate modeling of the scatter response; Record of the 1992 IEEE Nuclear Science Symposium and Medical Imaging Conference; 1992. p. 1035-1037.

Frey EC, Tsui BMW. A practical method for incorporating scatter in a projector-backprojector for accurate scatter compensation in SPECT. IEEE Trans Nucl Sci 1993;40:1107–1116.

Frey EC, Ju ZW, Tsui BMW. A fast projector-backprojector pair modeling the asymmetric, spatially varying scatter response function for scatter compensation in SPECT imaging. IEEE Trans Nucl Sci 1993;40:1992–1997.

Frey, EC.; Tsui, BMW. A new method for modeling the spatially-variant, object-dependent scatter response function in SPECT; Record of the 1996 IEEE Nuclear Science Symposium and Medical Imaging Conference; 1996. p. 1082-1086.

Hademenos GJ, Dahlbom M, Hoffman EJ. Simultaneous dual-isotope technetium-99*m*/thallium-201 cardiac SPET imaging using a projection-dependent spilldown correction factor. Eur J Nucl Med 1995;22:465–472. [PubMed: 7641755]

Hudson HM, Larkin RS. Accelerated image reconstruction using ordered subsets of projection data. IEEE Trans Med Imag 1994;13:601–609.

Johnson LL, Lerrick KS, Coromilas J, Seldin DW, Esser PD, Zimmerman JM, Keller AM, Alderson PO, Bigger JT, Cannon PJ. Measurement of infarct size and percentage myocardium infarcted in a dog preparation with single photon-emission computed tomography, thallium-201, and indium-111 monoclonal antimyosin Fab. Circulation 1987;76:181–190. [PubMed: 2439232]

Johnson LL, Seldin DW, Keller AM, Wall RM, Bhatia K, Bingham CO, Tresgallo ME. Dual-isotope thallium and indium antimyosin SPECT imaging to identify acute infarct patients at further ischemic risk. Circulation 1990;81:37–45. [PubMed: 2297842]

Juni JE, Bernstein RC, Ponto RA, Nuechterlein PM. Simultaneous dual-tracer brain SPECT with Tc-99*m* HMPAO and I-123 Iodoaphetamine-method and validation. J Nucl Med 1992;32:956P.

Kadrmas DJ, Frey EC, Tsui BMW. Analysis of the reconstructibility and noise properties of scattered photons in Tc-99*m* SPECT. Phys Med Biol 1997;42:2493–2516. [PubMed: 9434303]

Kadrmas DJ, Frey EC, Karimi SS, Tsui BMW. Fast implementations of iterative reconstruction-based scatter compensation in fully 3D SPECT image reconstruction. Phys Med Biol 1998a;43:857–873. [PubMed: 9572510]

Kadrmas DJ, Frey EC, Tsui BMW. Application of reconstruction-based scatter compensation to Tl-201 SPECT. IEEE Trans Med Imag 1998b;17:325–333.

Kamphuis C, Beekman FJ, van Rijk PP, Viergever MA. Dual matrix ordered subsets reconstruction for accelerated 3D scatter compensation in single-photon emission tomography. Eur J Nucl Med 1998;25:8–18. [PubMed: 9396869]

Kiat H, Germano G, Friedman J, Train KV, Silagan G, Wang FP, Maddahi J, Berman DS. Comparative feasibility of separate of simultaneous rest thallium-201 / stress technetium-99*m*-sestamibi dual-isotope myocardial perfusion SPECT. J Nucl Med 1994;35:524–528.

Klumper A, Zwijnenburg A. Dual isotope (81 Krm and 99Tcm) SPECT in lung function diagnosis. Phys Med Biol 1986;7:751–761. [PubMed: 3489241]

Knesaurek K. A new dual-isotope convolution cross-talk correction method: a Tl-201/Tc-99*m* SPECT cardiac phantom study. Med Phys 1994;21:1577–1583. [PubMed: 7869989]

Lange K, Carson R. E.M. reconstruction algorithms for emission and transmission tomography. J Comput Assit Tomog 1984;8:306–316.

Links JM, Prince JL, Gupta SN. A vector Wiener filter for dual-radionuclide imaging. IEEE Trans Med Imag 1996;15:700–709.

Liu P, Burns RJ, Houle S, Warbick-Cerone A, Johnston L, Gilday D, El-Maraghi N, Mclaughlin PR. Validation of cardiac single photon emission tomography of labeled intracoronary microspheres as a method to measure changes in distribution of coronary blood flow. Can J Cardiol 1986;6:362–367. [PubMed: 3492253]

Ljungberg M, Strand S-E. A Monte Carlo program for the simulation of scintillation camera characteristics. Comp Meth Prog Biomed 1989;29:257–272.

Lowe VJ, Greer KL, Hanson MW, Jaszczak RJ, Coleman RE. Cardiac phantom evaluation of simultaneously acquired dual-isotope rest thallium-201 / stress technetium-99*m* SPECT images. J Nucl Med 1993;34:1998–2006. [PubMed: 8229250]

Maddahi J, Rodrigues E, Berman DS, Kiat H. State-of-the-art myocardial perfusion imaging. Card Clin 1994;12:199–222.

Moore SC, Zimmerman RE, Chan KH, English RJ, Kijewski MF. Experimental and Monte Carlo characterization of spectral and spatial distributions of lead x-rays (abstract). J. Nucl. Med 1994;35:61P.

Moore SC, English RJ, Syravanh C, Tow DE, Zimmerman RE, Chan KH, Kijewski MF. Simultaneous Tc-99*m*/Tl-201 imaging using energy-based estimation of the spatial distribution of contaminant photons. IEEE Trans Nucl Sci 1995;42:1189–1195.

Neumann DR. Simultaneous dual-isotope SPECT imaging for the detection and characterization of parathyroid pathology. J Nucl Med 1992;33:131–134. [PubMed: 1730978]

O'Connor MK, Monville ME, Nonneman S. Development and validation of a Monte Carlo simulation of a gamma camera using MCNP (abstract). J. Nucl. Med 1998;39:97–98P.

Pretorius PH, Xia W, King MA, Tsui BMW, Pan TS, Villegas BJ. Evaluation of right and left ventricular volume and ejection fraction using a mathematical cardiac torso phantom for gated pool SPECT. J Nucl Med 1997;30:1528–1534. [PubMed: 9379187]

Sandrock D, Merino MJ, Norton JA, Neumann RD. Parathyroid imaging by Tc/Tl scintigraphy. Eur J Nucl Med 1990;16:607–613. [PubMed: 2166664]

Shepp LA, Vardi Y. Maximum likelihood estimation for emission tomography. IEEE Trans Med Imag 1982;1:113–121.

Terry, JA.; Tsui, BMW.; Perry, JR.; Hendricks, JL.; Gullberg, GT. The design of a mathematical phantom of the upper human torso for use in 3-D SPECT imaging research; Proceedings of the 1990 Fall Meeting of the Biomedical Engineering Society; Blacksburg: Biomedical Engineering Society; 1990. p. 1467-1474.

Tsui BMW, Zhao XD, Gregoriou GK, Lalush DS, Frey EC, Johnson RE, McCartney W. Quantitative cardiac SPECT reconstruction with reduced image degradation due to patient anatomy. IEEE Trans Nucl Sci 1994;41:2838–2844.

Welch A, Gullberg GT, Christian PE, Datz FL. A transmission map-based scatter correction technique for SPECT in inhomogenous media. Med Phys 1995;22:1627–1635. [PubMed: 8551987]

Yang DC, Ragasa E, Gould L, et al. Radionuclide simultaneous dual-isotope stress myocardial perfusion study using the "three window technique". Clin Nucl Med 1993;18:852–857. [PubMed: 8242977]

Zar, JH. Biostatistical Analysis. Upper Saddle River, NJ: Prentice-Hall, Inc; 1996.

Zeng GL, Gullberg GT. Frequency domain implementation of the three-dimensional geometric point source correction in SPECT imaging. IEEE Trans Nucl Sci 1992;39:1444–1453.

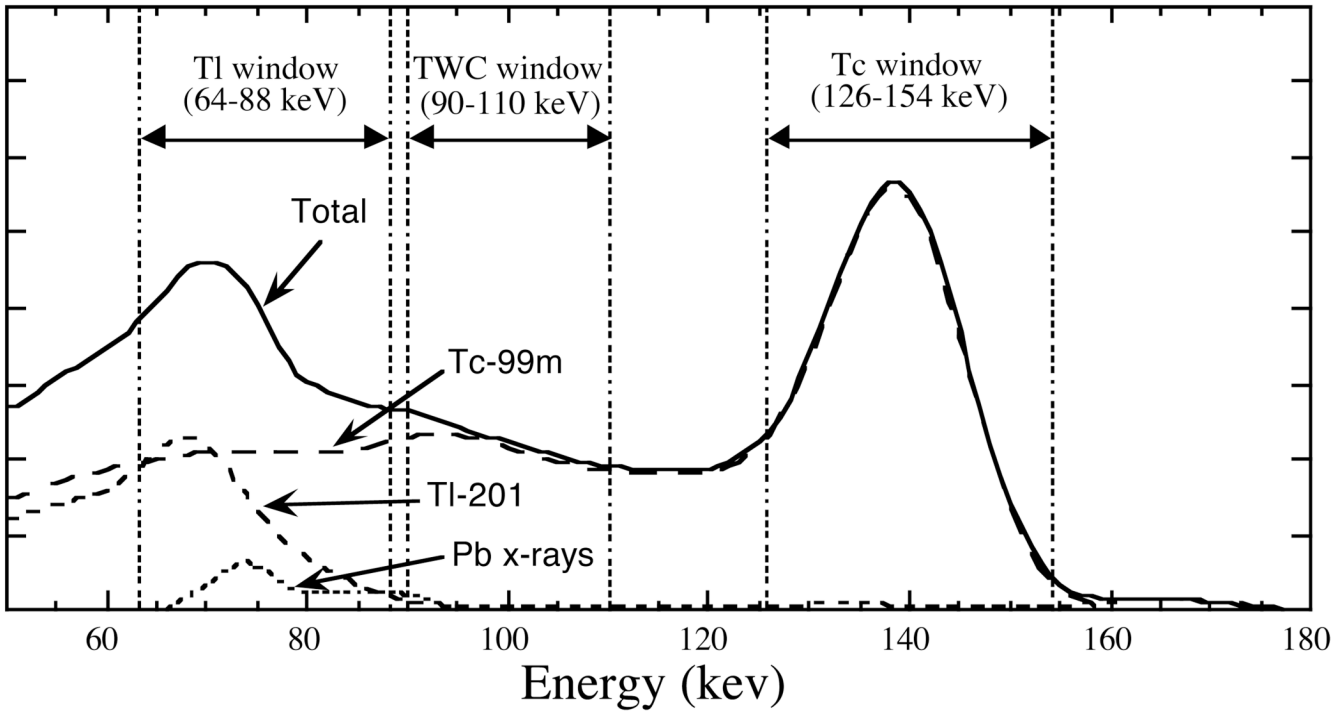

Figure 1.
Sample dual-isotope energy spectrum indicating the components due to Tc-99*m*, Tl-201, and lead fluorescence x-rays (from Tc-99*m* photons interacting with the collimator). Photopeak energy windows for Tc and Tl are indicated, and the third energy window used by the TWC compensation method is also shown.

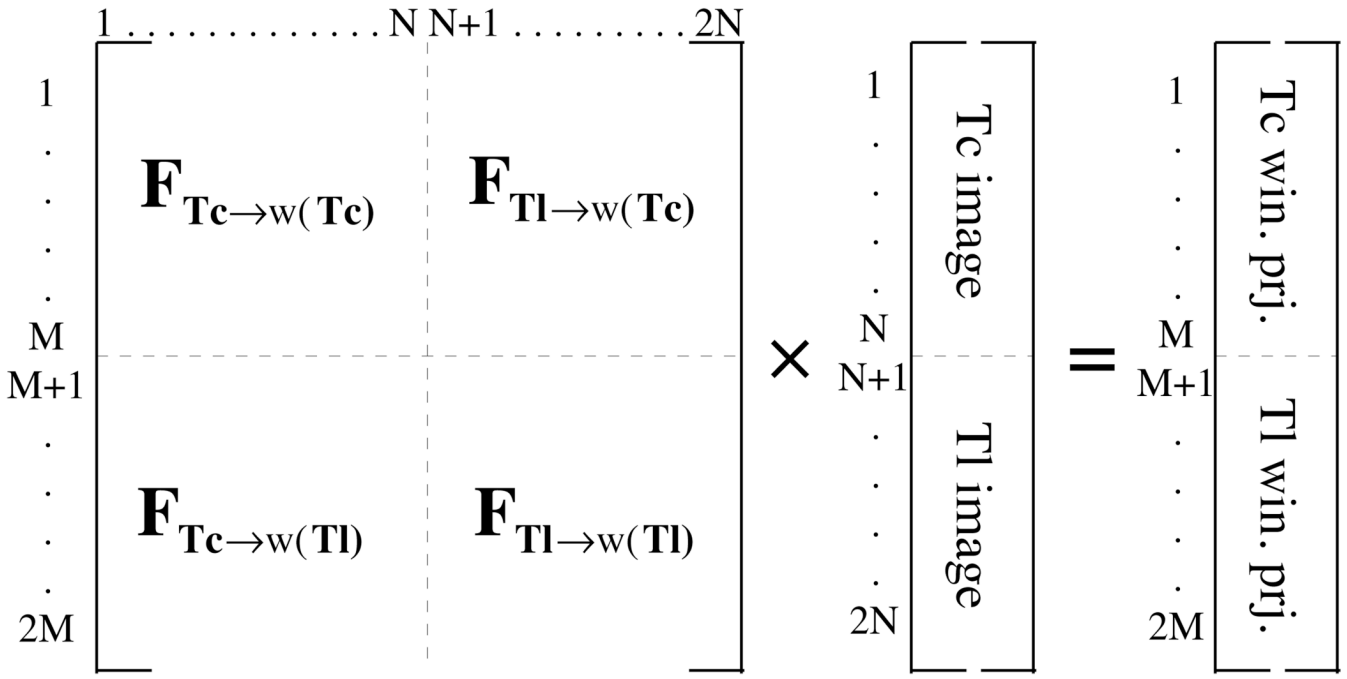

Figure 2.
Diagrammatic representation of the imaging equation for the SimMBC method. Each quadrant of the projection matrix describes the projection of the image for a single isotope into one of the energy windows. All the physics of the projection process, including self-scatter and cross-talk, are included in the projection matrix.

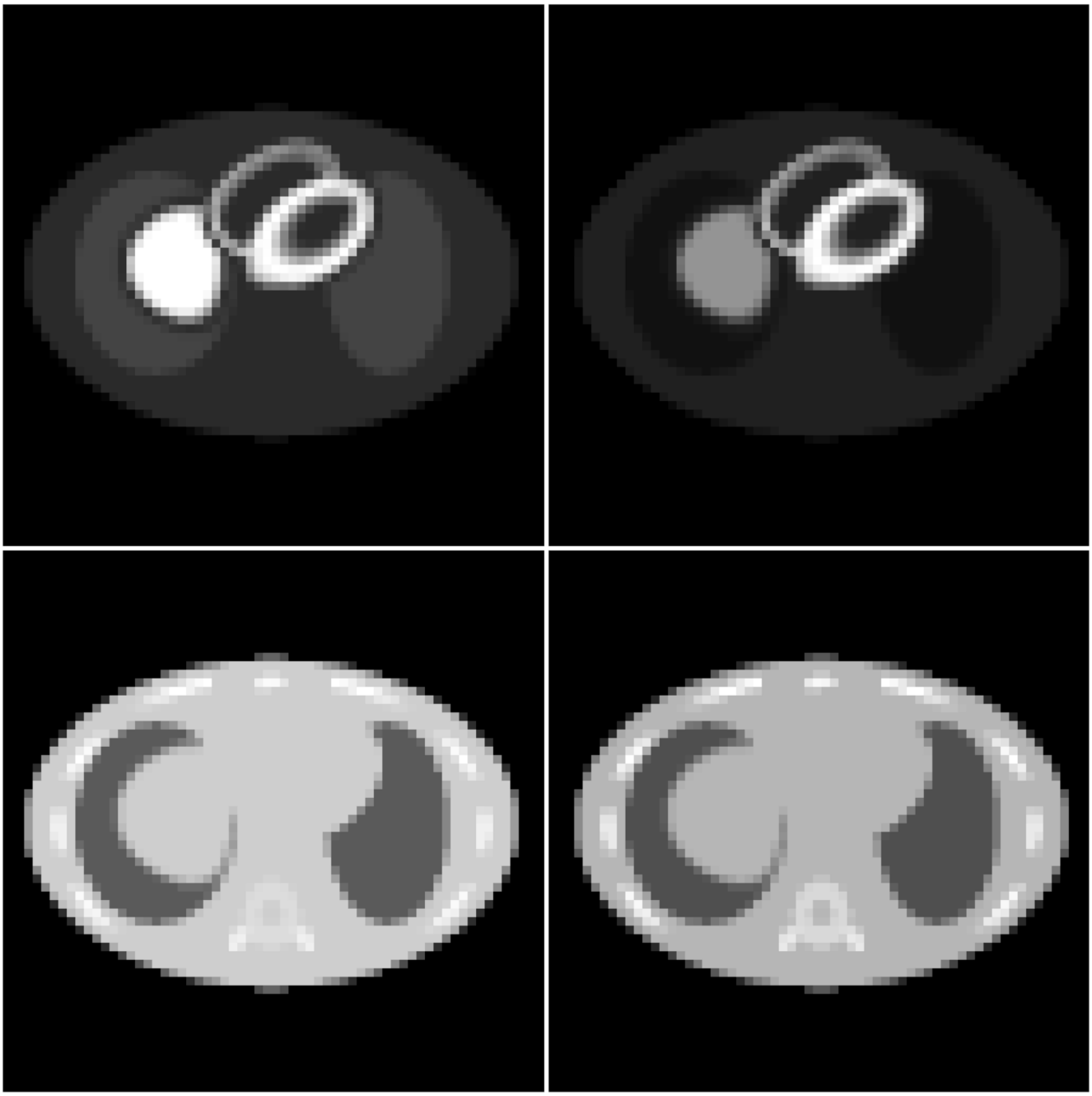

Figure 3.
Sample slices of the MCAT phantom activity distributions (top row) and attenuation maps (bottom row). The Tc-99*m* sestamibi phantom is shown on the left, and the Tl-201 phantom is on the right.

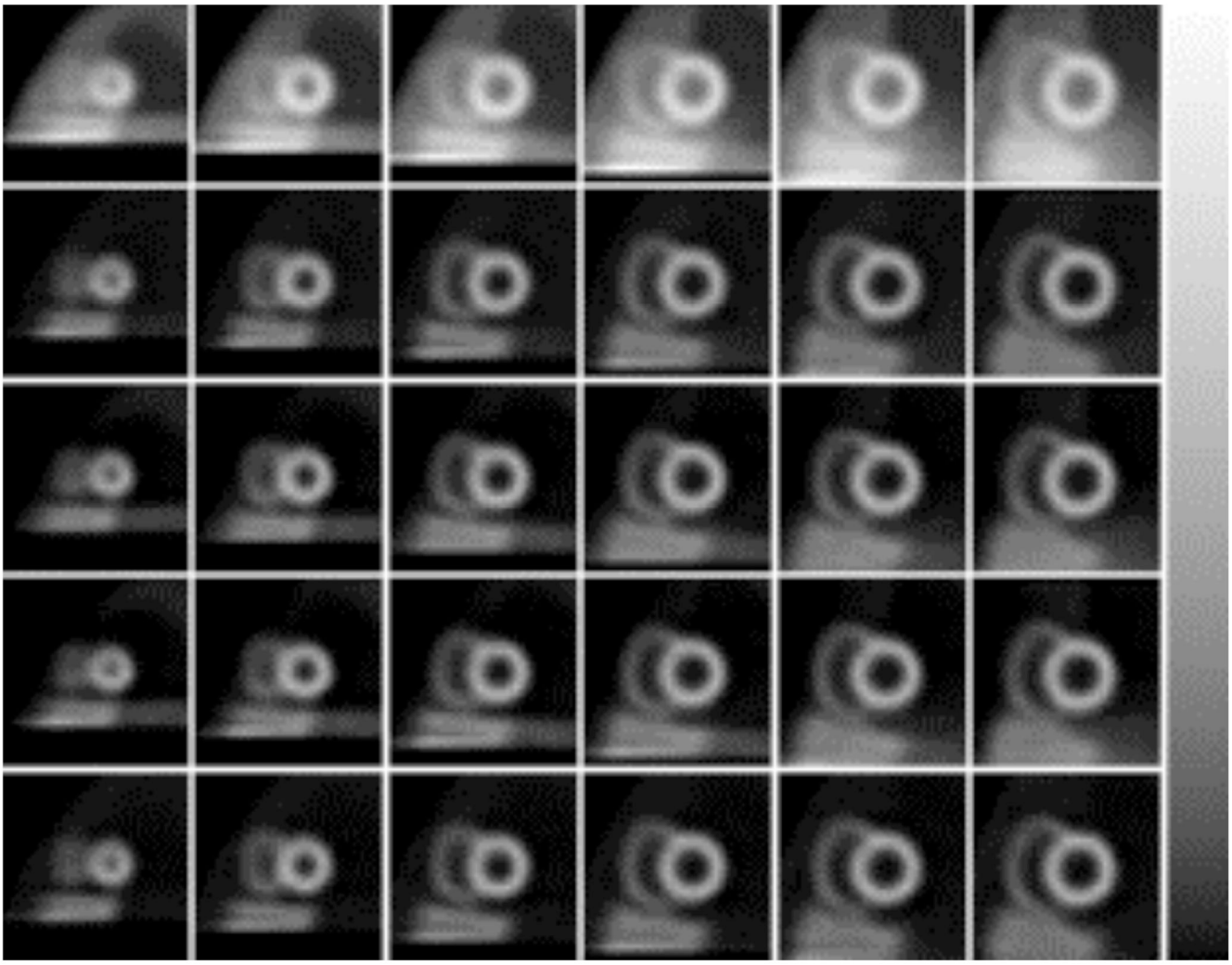

Figure 4.
Reconstructed Tl short axis slices for the noise-free simulated MCAT projection data (top row to bottom row): no compensation, TWC, SimMBC, SeqMBC, and no cross-talk. All image were displayed using the same grayscale, shown at the right.

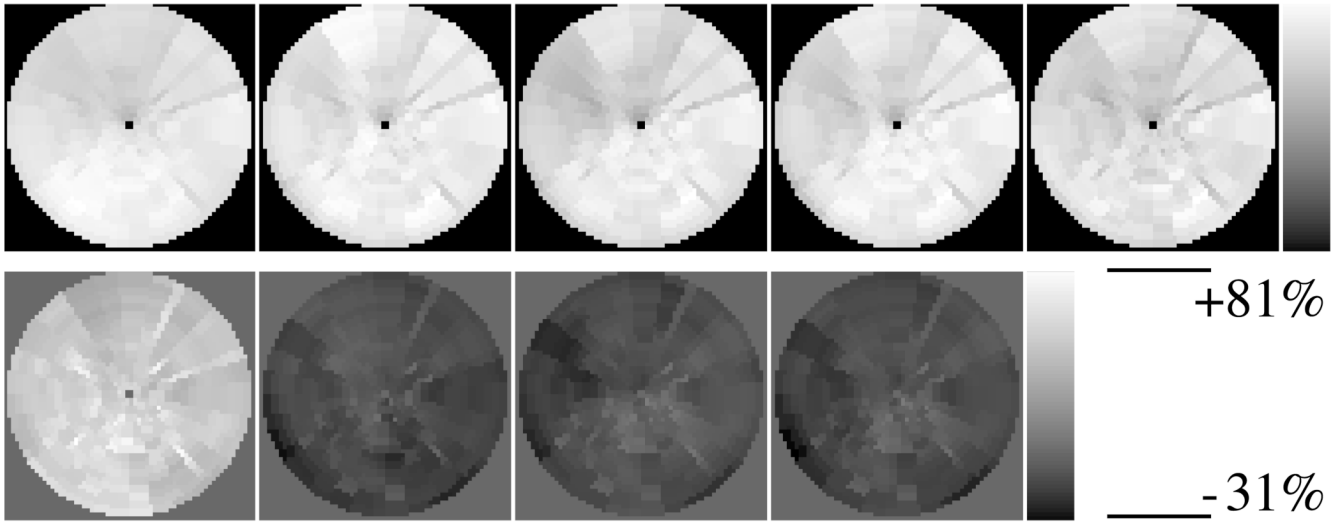

Figure 5.
Polar maps (top row) and relative error polar maps (bottom row) for the noise-free Tl MCAT reconstructions and the cases of (left to right): no compensation, TWC, SimMBC, SeqMBC, and no cross-talk. The relative error polar maps are displayed as percent error relative to the no cross-talk polar map.

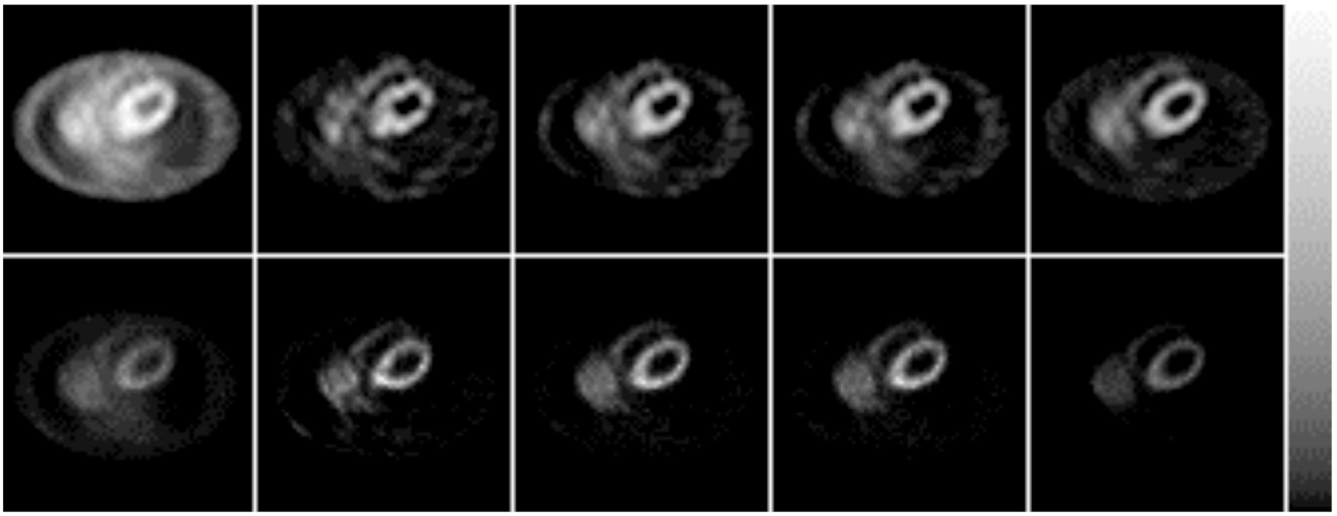

Figure 6.
Reconstructed transaxial Tl images from noisy data (top row) and reconstructed variance images (bottom row) for the cases of (left to right): no compensation, TWC, SimMBC, SeqMBC, and no cross-talk. All images were displayed using the grayscale shown at the right.

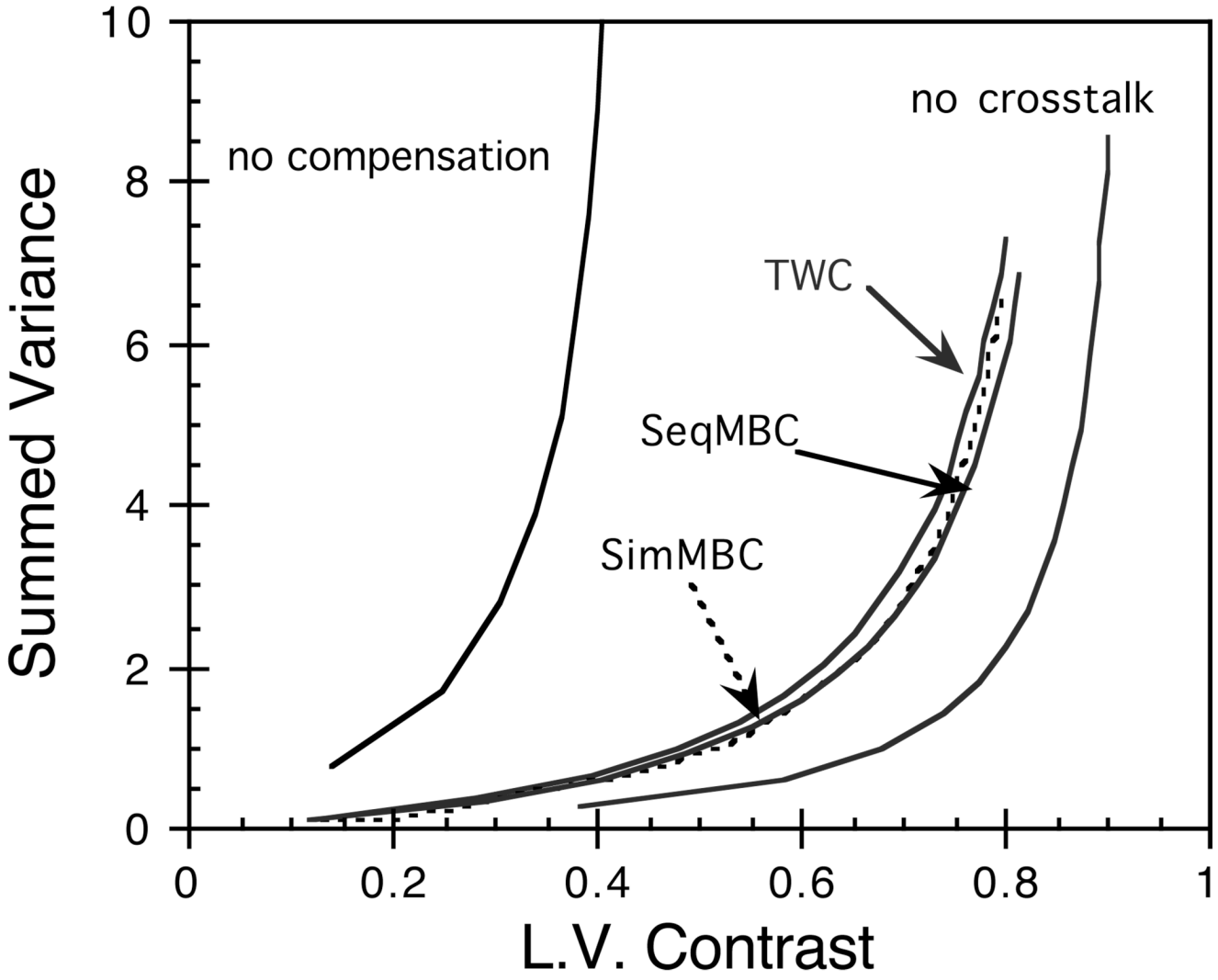

Figure 7.
Sum of the pixels in the reconstructed Tl variance images plotted versus left ventricle contrast ratio. Plotting versus contrast instead of iteration helps ensure a meaningful comparison can be made.

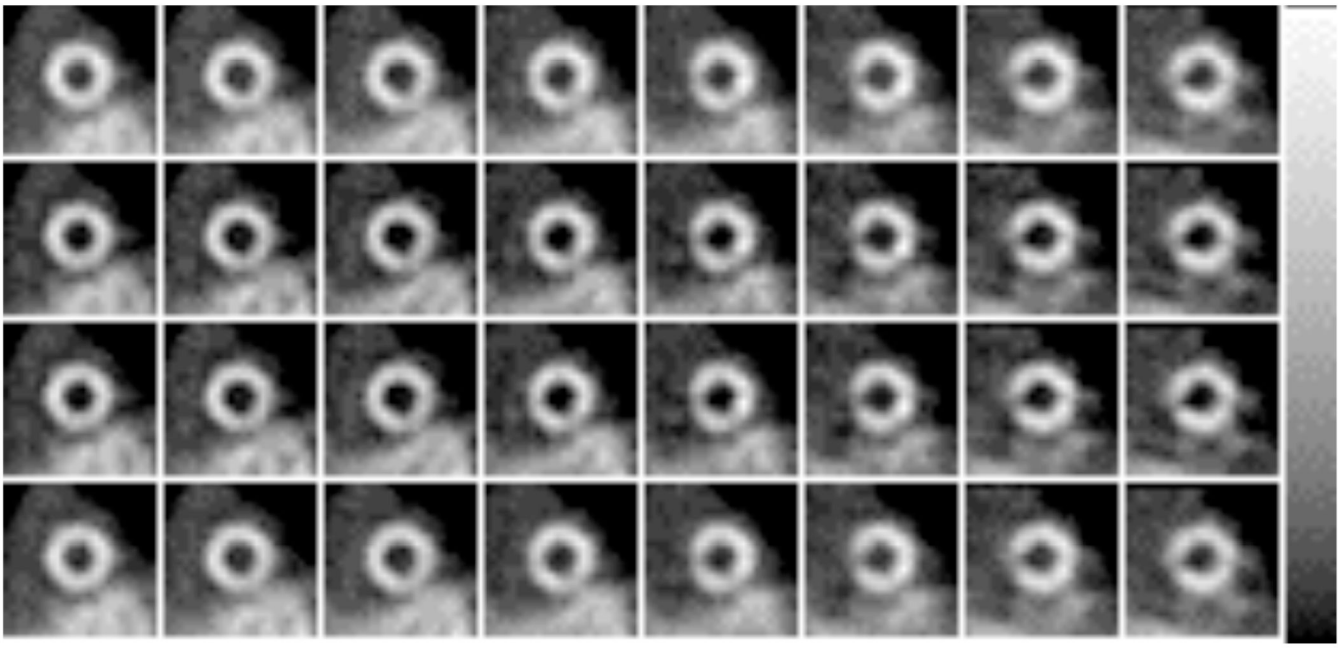

Figure 8.
Reconstructed short-axis Tc images for the anthropomorphic phantom experiment: no cross-talk compensation (top row), compensated with the SimMBC method without (2nd row) and with (3rd row) the preliminary model for collimator interactions, and separately acquired ‘no cross-talk’ image (bottom row). The lesion in the basal septal wall is clearly visible for all cases. All images were displayed with the same grayscale, shown at the right.

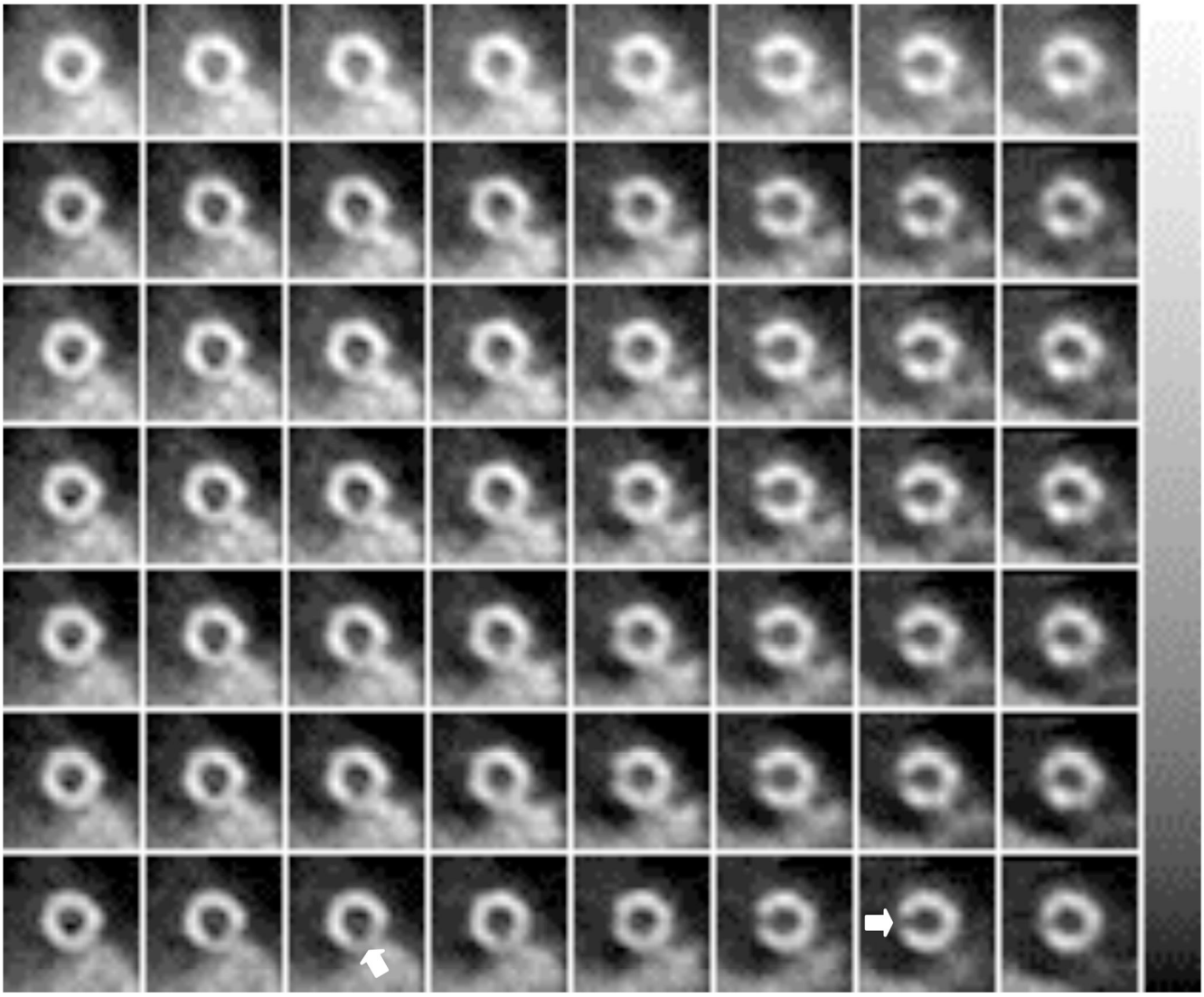

Figure 9.
Reconstructed short-axis Tl images for the anthropomorphic phantom experiment for the cases of (from top to bottom): no cross-talk compensation, TWC, SimMBC without x-ray model, SimMBC with x-ray model, SeqMBC without x-ray model, SeqMBC with x-ray model, and 'no cross-talk' image. The approximate positions of the lesions are indicated on the 'no cross-talk' images. All images were displayed using the same grayscale, shown at the right.

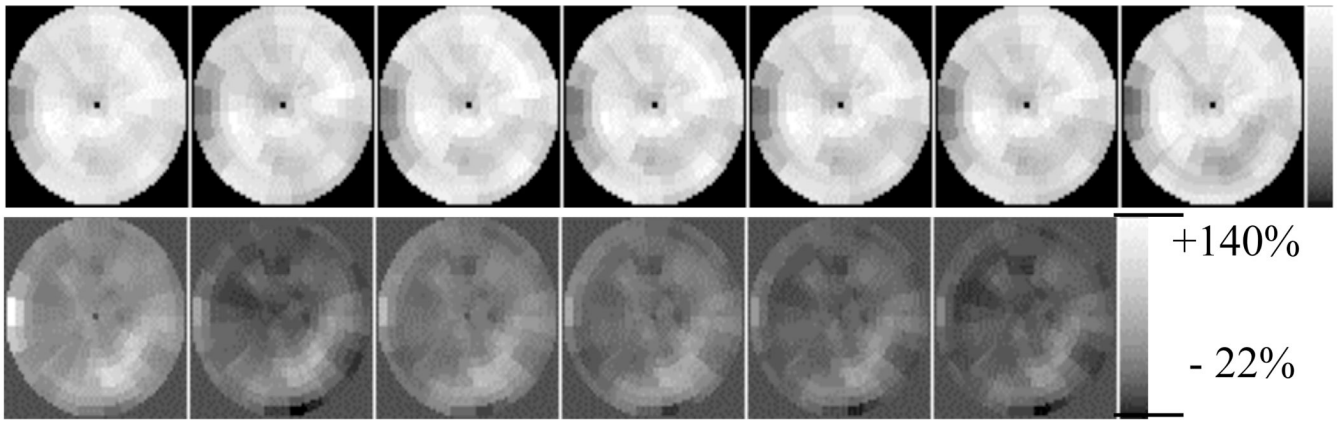

Figure 10.
Polar maps (top row) and relative error polar maps (bottom row) corresponding to the images shown in Figure 9 (from left to right): no cross-talk compensation, TWC, SimMBC without x-ray model, SimMBC with x-ray model, SeqMBC without x-ray model, SeqMBC with x-ray model, and 'no cross-talk' image. The polar maps on the bottom row are displayed as percent error relative to the 'no cross-talk' polar map.

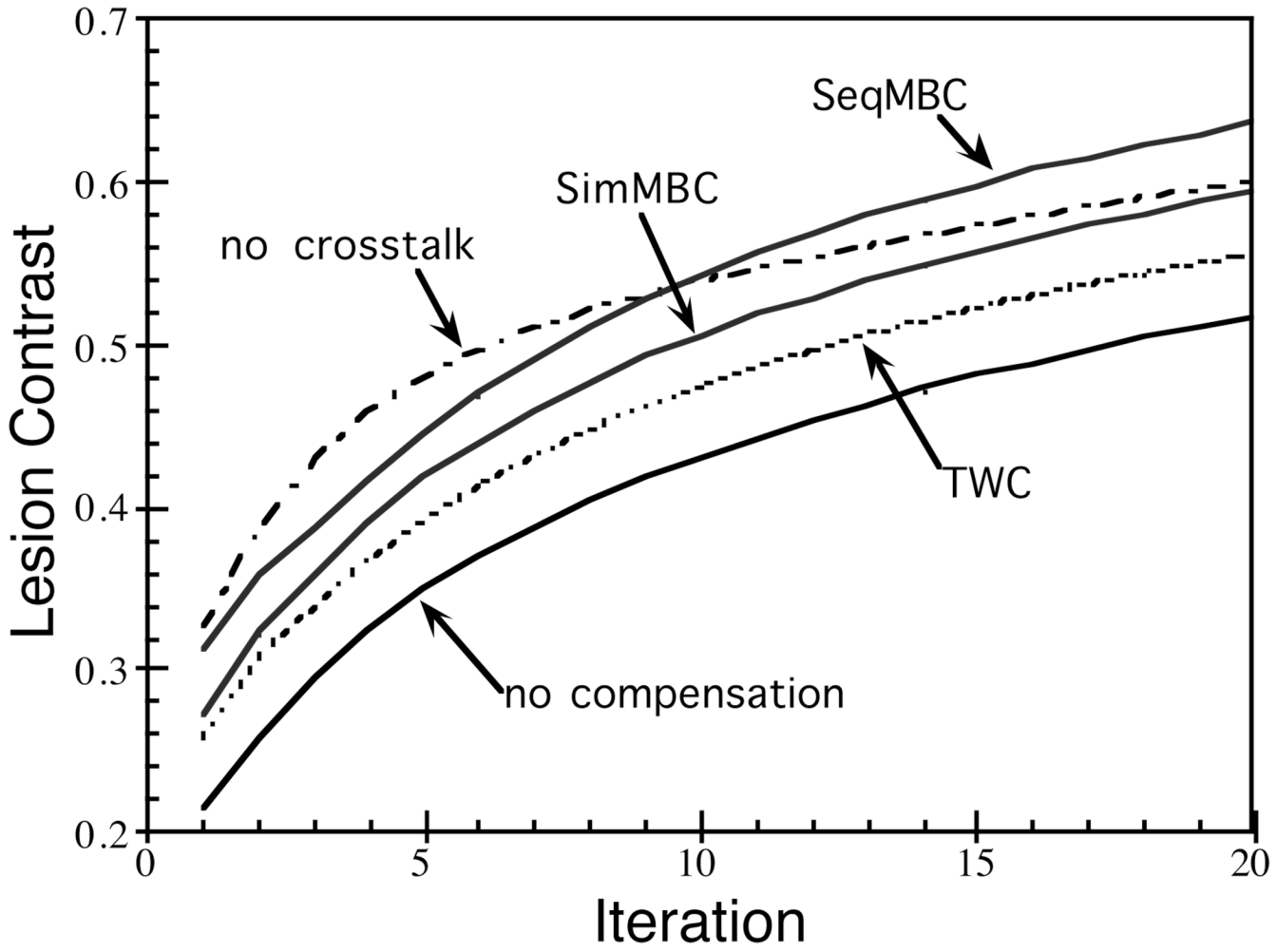

Figure 11.
Contrast of the Tl lesion placed in the basal septal wall plotted versus iteration number. The SimMBC and SeqMBC methods included the preliminary model for collimator interactions.